ACS Sustainable Chemistry & Engineering

Research Article

Cite This: ACS Sustainable Chem. Eng. 2019, 7, 5875−5885

pubs.acs.org/journal/ascecg

OX-1 Metal−Organic Framework Nanosheets as Robust Hosts for Highly Active Catalytic Palladium Species

Kirill Titov,[†,⊥] Dmitry B. Eremin,[‡,⊥] Alexey S. Kashin,[‡] Roberto Boada,[§] Barbara E. Souza,[†] Chris S. Kelley,[§] Mark D. Frogley,[§] Gianfelice Cinque,[§] Diego Gianolio,[§] Giannantonio Cibin,[§] Svemir Rudić,[∥] Valentine P. Ananikov,[*,‡] and Jin-Chong Tan[*,†]

[†]Multifunctional Materials & Composites (MMC) Laboratory, Department of Engineering Science, University of Oxford, Parks Road, Oxford OX1 3PJ, United Kingdom

[‡]Zelinsky Institute of Organic Chemistry, Russian Academy of Sciences, Leninsky Pr. 47, Moscow 119991, Russia

[§]Diamond Light Source, Harwell Campus, Chilton, Didcot OX11 0DE, United Kingdom

[∥]ISIS Facility, STFC, Rutherford Appleton Laboratory, Chilton, Didcot OX11 0QX, United Kingdom

Supporting Information

ABSTRACT: A catalytic system based on OX-1 metal−organic framework nanosheets is reported, incorporating catalytically active palladium (Pd) species. The Pd@OX-1 guest@host system is rapidly synthesized via a one-step single-pot supramolecular assembly, with the possibility of controlling the Pd loading. The structures of the resulting framework and of the active Pd species before and after catalytic reactions are studied in detail using a wide variety of techniques including synchrotron radiation infrared spectroscopy, inelastic neutron scattering, and X-ray absorption spectroscopy. Crystals of the resulting Pd@OX-1 composite material contain predominantly atomic and small cluster Pd species, which selectively reside on benzene rings of the benzenedicarboxylate (BDC) linkers. The composites are shown to efficiently catalyze the Suzuki coupling and Heck arylation reactions under a variety of conditions. Pd@OX-1 further shows potential to be recycled for at least five cycles of each reaction as well as an ability to recapture active Pd species during both catalytic reactions.

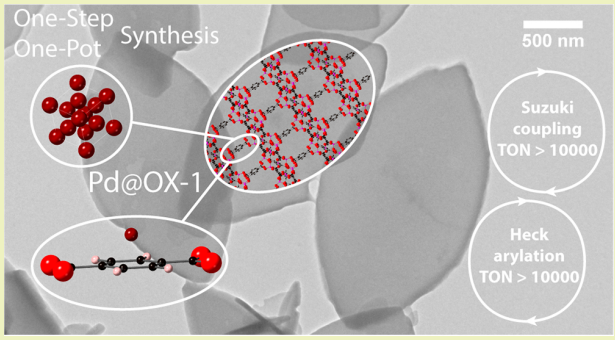

KEYWORDS: *Nanosheets, Metal−organic framework, Palladium, Catalysis, Inelastic scattering*

INTRODUCTION

The vast chemical and physical versatility of metal−organic framework (MOF) materials opens the door to a range of potential technological applications: adsorption, catalysis, charge transport and luminescence, photonics and chemical sensing, and delivery of functional guest molecules.[1,2] There has been mounting interest in the exploration of MOF compounds or MOF-based composites to afford heterogeneous catalysis, summarized by recent reviews in this topic area.[3−6] Interesting findings include the demonstration that the activity of MOF catalysts containing coordinatively unsaturated sites, such as UiO-66, can be significantly enhanced by functionalized linkers.[7] A related study shows that catalytic activity of MIL-100(Fe) can be substantially enhanced and tuned by introducing defects in the structure via acid pretreatment.[8] In the study of MOF-based composites as catalysts, an emerging avenue involves the immobilization of fine-scale metal nanoparticles confined in the high-surface-area MOF hosts,[9] yielding bespoke composites exhibiting a good combination of chemical and mechanical properties.[10]

Metal−organic nanosheets[11,12] and hybrid nanoplate structures[13] present a two-dimensional (2D) platform not only for engineering thin-film devices[14,15] but also showing promise for photocatalytic applications.[16] Recently, we have discovered a porous Zn-based nanosheet structure designated as OX-1 for "Oxford University-1 material" [$(Et_3NH)_2Zn_3BDC_4$; Et_3N = triethylamine, BDC = 1,4-benzenedicarboxylate], which may serve as an efficient host structure to confine (guest) luminescent metal complexes.[17] It demonstrated the interesting concept of guest@MOF (host) strategy,[18] enabled by a rapid one-pot supramolecular assembly approach under ambient conditions. It is envisaged that this guest@MOF strategy may be extended to achieve the *in situ* encapsulation of fine-scale metal nanoparticles as catalytically active species.

The catalytic formation of C−C bonds is considered to be one of the key transformations in organic synthesis.[19] The use

Received: November 9, 2018
Revised: February 1, 2019
Published: February 20, 2019

DOI: 10.1021/acssuschemeng.8b05843
ACS Sustainable Chem. Eng. 2019, 7, 5875−5885

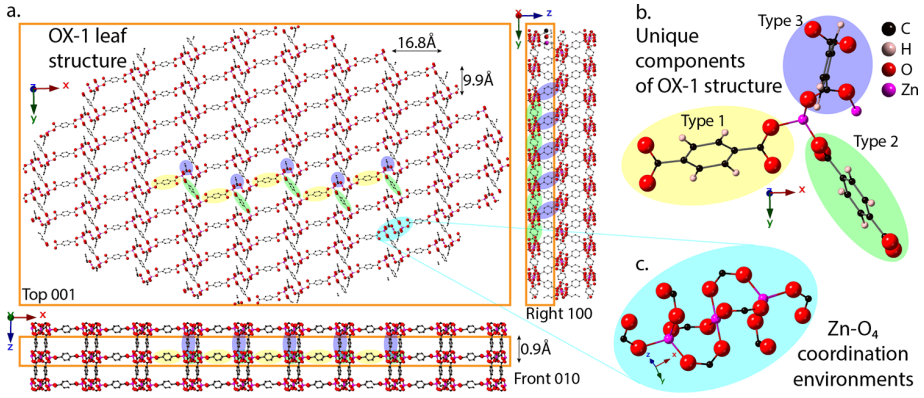

Figure 1. Crystal structure of OX-1 nanosheets exhibiting a leaf-shaped morphology: (a) views of a selected 2D layer (bound by the orange box) making up the 3D sheet structure; (b) details of the unique components of the structure—2 unique Zn centers and 3 possible orientations of BDC linker; (c) detail of the Zn coordination environments. Colored ovals highlight the positions of the different types of structural motifs.

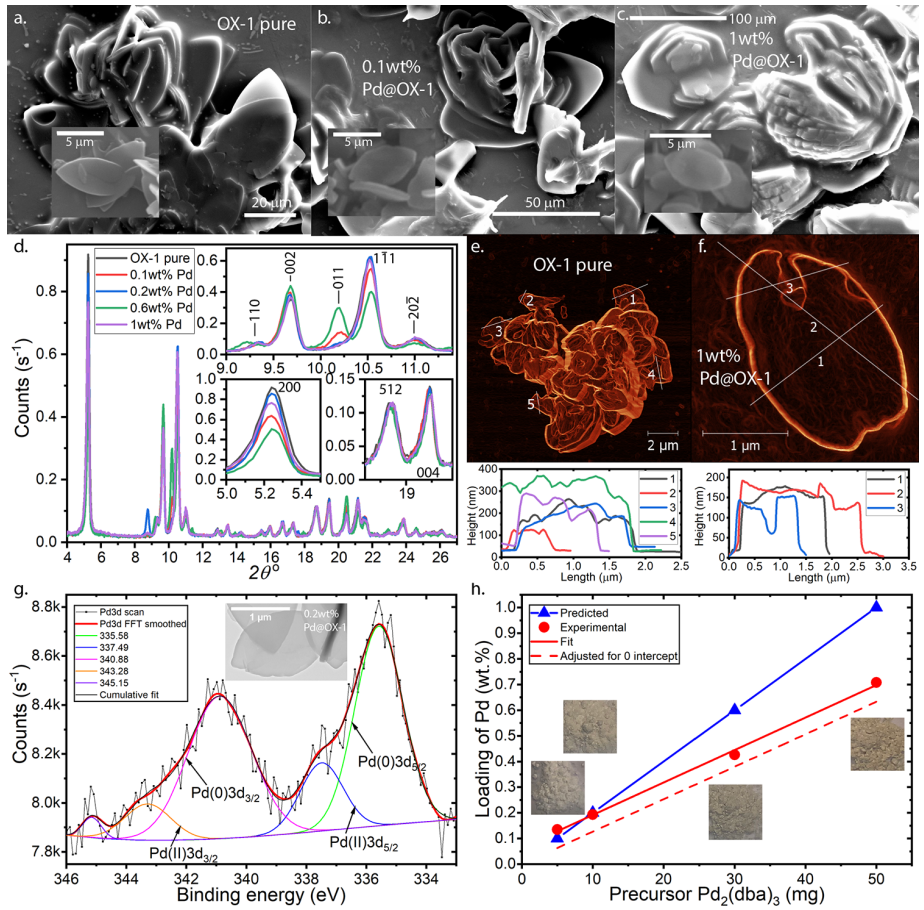

Figure 2. OX-1 and Pd@OX-1 crystals: SEM (a–c) and AFM images (e, f) of pure OX-1 (a, e) and Pd@OX-1 (b, c, f); PXRD patterns (d) of a series of Pd@OX-1 materials with different Pd loadings; XPS spectrum (g) of the 0.2 wt % Pd@OX-1 with a TEM image of the crystal inset; theoretical and experimental Pd content in Pd@OX-1 measured by XRF (h) for the sample series in (d), with photos of the respective powders.

of transition metals as catalysts for these transformations is a vibrant area of research, especially involving metal nanoparticles.[20−25] The precise processes involved in nanoparticle catalysis are a matter of ongoing investigations,[26] while the ultimate aim is the rational design of efficient, selective and stable catalysts, with an awareness of the dynamic evolution of the active species during catalysis.[26−30]

MOF materials possess unique properties, such as tunable porosity and the ability to fine-tune the structure of the active sites and their environments,[31] which can be utilized in achieving the above aims. MOF catalytic activity can be achieved via three main routes: activity at the inorganic nodes and the organic, or pseudo-organic, linkers of the framework itself; encapsulation of active species into the framework; and

DOI: 10.1021/acssuschemeng.8b05843
ACS Sustainable Chem. Eng. 2019, 7, 5875−5885

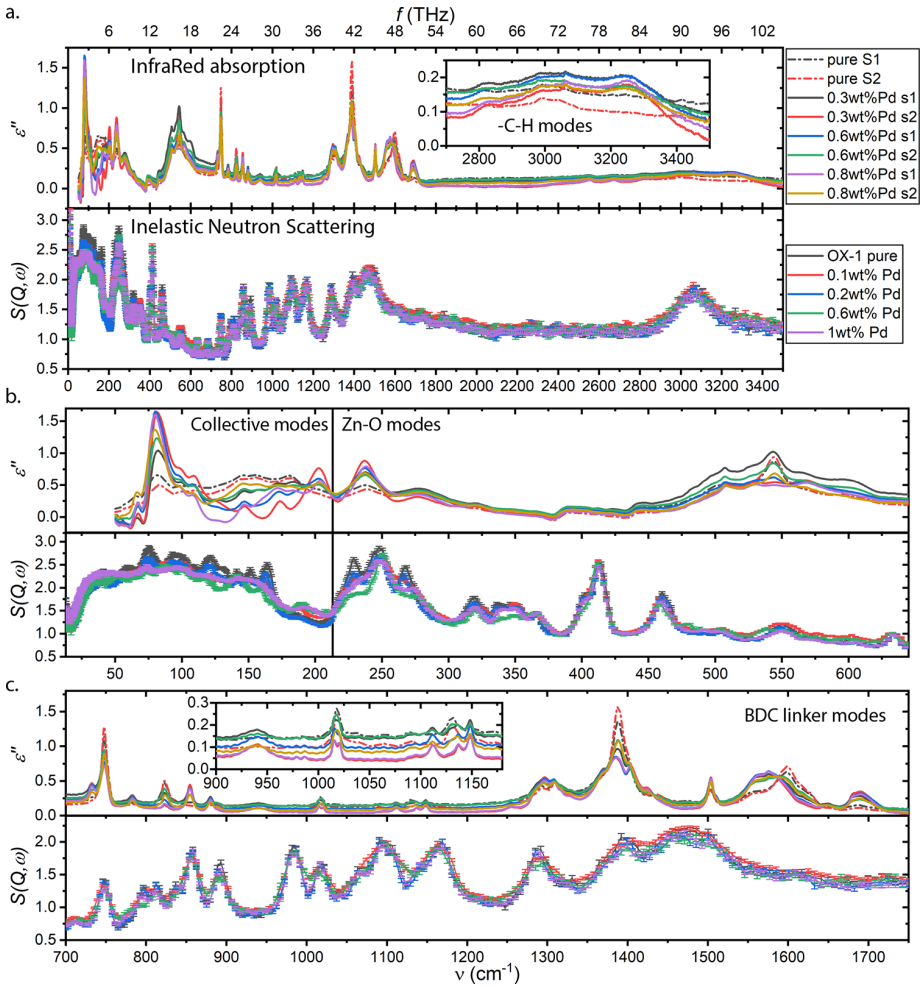

Figure 3. Infrared absorption spectra (top of each panel) and inelastic neutron scattering spectra (bottom of each panel) of Pd@OX-1 materials with various Pd loadings. These measurements were carried out on two separately synthesized series of materials for two separate beam times.

postsynthetic modification of the framework.[31−35] Some notable examples of catalytic MOFs for C−C bond formation so far have been achieved through encapsulation of active palladium (Pd) species into the MIL family of MOFs,[34,36−41] as well as UiO-66,[42] UiO-67,[43] MIL-53(Al)-NH_2,[44] ScBTC NMOF,[45] $Cu_2(BDC)_2DABCO$,[46] and MOF-5.[47] These materials have been shown to catalyze the Suzuki reaction for a wide range of substrates, but few demonstrate catalysis of the Heck reaction.[40,44] However, these MOFs are difficult and resource-intensive to synthesize, often requiring prolonged heating in autoclave enclosures, and in all cases requiring a long secondary processing step to incorporate the active Pd phase into the framework. The present work adddresses these difficulties without compromising the high activity at low loadings of incorporated Pd species.

In this study we report a new catalytic system based on OX-1 nanosheets, incorporating catalytically active Pd species. The Pd@OX-1 guest@host system is rapidly synthesized via a one-step single-pot supramolecular assembly, with the possibility of controlling the Pd loading. The structures of the resulting framework and of the active Pd species before and after catalytic reaction are studied in detail using a wide variety of techniques including synchrotron radiation infrared (SRIR) spectroscopy, inelastic neutron scattering (INS), and X-ray absorption spectroscopy (XAS). Pd@OX-1 is shown to be a highly efficient catalyst of the Suzuki coupling and Heck arylation reactions, with the possibility of recycling the material for at least five cycles of each reaction. Furthermore, OX-1 is shown to possess active sites for Pd attachment, which are not deactivated in the process of the Heck reaction and even survive a complete transformation of crystal structure during the Suzuki reaction.

EXPERIMENTAL SECTION

Materials Synthesis. We synthesized a series of OX-1 materials with varying loadings of palladium (Pd), whose zero valency form, Pd(0), is an active catalyst for a variety of important organic synthesis reactions. Palladium is embedded in the material during OX-1 synthesis and does not affect the processing time. To incorporate 0.1−1 wt % of Pd into OX-1, 5−50 mg of the precursor $Pd_2(dba)_3$ complex [dba = dibenzylideneacetone] was dissolved in 2 mL of DMF and added to 3 mmol of benzene-1,4-dicarboxylic acid and 6 mmol of Et_3N in 3 mL of DMF. This mixture was then combined with 1.5 mmol of $Zn(NO_3)_2$ in 2 mL of DMF, at which stage a gel was observed and OX-1 crystals were formed. The gel was then transferred to a 50 mL centrifuge tube, with 43 mL of DMF added in the process. This mixture was sonicated until it lost its pink color, becoming gray-greenish. It was then centrifuged for 5 min at 8000 rpm, to separate the light gray crystals from the light marsh solution of dba and excess BDC in DMF. The crystals were then washed twice in acetone and

DOI: 10.1021/acssuschemeng.8b05843
ACS Sustainable Chem. Eng. 2019, 7, 5875−5885

dried overnight at 100 °C (yield ~500 mg). The color change from pink to green-gray during the first sonication step is evidence of dissociation of the Pd complex. During this step Pd atoms break free of the $Pd_2(dba)_3$ complex and bind onto OX-1. Gas chromatography−mass spectrometry (GC-MS) and ^1H nuclear magnetic resonance (NMR) spectroscopy measurements were carried out to confirm the presence of free dba in solution, showing that Pd has been dissociated from the $Pd_2(dba)_3$ complex. It is important to note that it was not possible to reproduce the Pd@OX-1 material by dispersing presynthesized OX-1 crystals in DMF, adding only $Pd_2(dba)_3$ to the mixture and sonicating—in this case the white OX-1 turned black, indicating that large Pd particles formed over an extended period of suspension in DMF. Details of the characterization methods employed in this study are presented in the Supporting Information (SI).

RESULTS AND DISCUSSION

Crystal Structure and Scalability. The OX-1 crystal structure,[17] shown in Figure 1, gives rise to a 3D leaf-shaped sheet formation in a one-pot supramolecular synthesis. Single layers of Zn metal centers and BDC linkers (Figure 1a) are stacked with an offset of half pore width and a reflection to create the sheets seen in Figure 2a−c, e, f. This structure is built up using just five unique components (see Figure 1b): two different Zn centers and three different orientations of BDC linkers. Type 1 linkers connect the metal nodes along the *x*-axis, and type 2 linkers connect the metal nodes along the *y*-axis—together they create the 2D layers of the structure. Type 3 linkers act as spacers and cross-bracing between the 2D layers. Each metal node (see Figure 1c) is made of three Zn centers, to which eight BDC linkers are coordinated. Two of the Zn centers have tetrahedral coordination environments, and one has a square planar coordination environment.

OX-1 is a highly attractive material for practical applications: the rapid high yield synthesis route (detailed above) is readily scaled—while the nominal reported yield is about 500 mg, as much as 3 g of OX-1 powder was obtained from a single reaction as part of this work with an insignificant increase in processing time. Moreover, OX-1 is readily functionalized: guest species can be incorporated via the same single pot method. The possibility of pelletizing OX-1, and its functionalized variants, without loss of crystallinity, is also shown in this work, making it even more practicable (see specular reflection IR methods in SI).

Capture of Pd onto OX-1 Active Sites. The chemical reaction described above produced leaf-shaped crystals with sizes varying between 5 and 100 μm in length and between 100 nm and 2 μm in thickness. Figure 2a−c shows SEM images of pure OX-1 crystals and Pd@OX-1 crystals, while Figure 2e, f shows AFM images with an edge detection filter applied and some extracted height profiles. These show that the smaller crystals do not change morphology when increasing amounts of precursor $Pd_2(dba)_3$ complex are added to the gel synthesis. The larger crystals, however, undergo a change: Figure 2c shows that the shape of the leaves changes to a more hexagonal geometry and additional smaller layers are seen appearing on top of the large plates upon introduction of 50 mg of $Pd_2(dba)_3$ into the reaction gel. These changes in morphology are captured by the X-ray diffraction (XRD) patterns shown in Figure 2d. The numbers of Bragg reflections between various crystallographic planes changes, seen most strikingly in the changing magnitude of the 5.25° peak corresponding to the (200) crystallographic planes, but the distances between planes do not change because the peaks do not shift to higher or lower angles. The presence of Pd thus does not distort the underlying structure of host OX-1 crystals, but the presence of $Pd_2(dba)_3$ in the gel during synthesis affects their morphology. X-ray photoelectron spectroscopy (XPS) measurement (Figure 2g) of 0.2 wt % Pd@OX-1 (used for all catalysis experiments in this study) reveals the predominance of Pd(0) phase of palladium in the material. X-ray fluorescence spectroscopy (XRF) measurements (Figure 2h) of a series of variously loaded Pd@OX-1 crystals reveal a linear relationship between the amount of $Pd_2(dba)_3$ added to the reaction gel and the amount of Pd detected in the washed and dried product.

Figure 3 shows infrared (IR) absorption spectra derived from specular reflectance measurements of pelletized Pd@OX-1 samples via a Kramers−Kronig transformation.[48] This method of IR spectroscopy provides information on IR active vibrational modes of compounds near the surface of the samples, with depth of penetration of IR beam being material dependent and not easily determined. These IR measurements were performed at the MIRIAM (B22) beamline of the Diamond Light Source synchrotron. Figure 3 also shows inelastic neutron scattering (INS) spectra taken at the TOSCA beamline of ISIS neutron source. INS is a highly penetrating nonselective technique, which provides information on all vibrational modes of the sample (no optical selection rule), probing the whole volume of the material and thus averaging across all local environments and especially sensitive to modes involving hydrogen motions.

The modes probed in IR absorption spectra are all detected in INS spectra, but the relative intensities of those peaks do not match. Furthermore, INS spectra also contain IR inactive modes. The spectra for the pristine OX-1 material thus resemble each other but do not match exactly, which might be due to the different penetration depth and selection rules for the two techniques. When Pd is introduced, dramatically different changes are observed by the two methods, which emphasizes the complementarity of IR and INS spectroscopies.

Ab initio density functional theory (DFT) calculations for a very similar material, MOF-5, were reported by Civalleri and co-workers[49] and can serve as a rough guide for vibrational mode assignment in spectra for OX-1. As indicated in Figure 3, collective modes of the framework are present below 200 cm^{-1}, various Zn−O bond modes appear between 200 and 650 cm^{-1}, and the various modes of BDC linkers, or their components, appear above 700 cm^{-1}. Both IR and INS spectra show significant changes in collective modes and Zn−O bond modes, but only IR spectra show noticeable changes in the BDC linker modes. Closer examination also reveals that the changes below 700 cm^{-1} are different for IR and INS spectra. IR reveals a dramatic enhancement of the collective mode at 80 cm^{-1}, and noticeable enhancement of bands at 200 and 280 cm^{-1}. INS spectra, on the other hand, show dampening of most collective modes up to 175 cm^{-1}, as well as the sidebands of the triple peak in the region 213−280 cm^{-1}. The BDC linker modes are also affected differently. IR spectra show dramatic changes in practically all BDC modes, whereas INS spectra show minor changes, which are difficult to attribute to introduction of Pd in the sample. Moreover, none of the changes in IR spectra appear to scale with amount of Pd loaded into the samples. This is most clearly seen in the shift of peaks from around 1600 cm^{-1} down to about 1575 cm^{-1}: all studied loadings appear to have the same step-like effect. However, the changes in INS spectra appear to follow the same trend as the changes in magnitudes of XRD peaks, most notably the (200)

DOI: 10.1021/acssuschemeng.8b05843
ACS Sustainable Chem. Eng. 2019, 7, 5875−5885

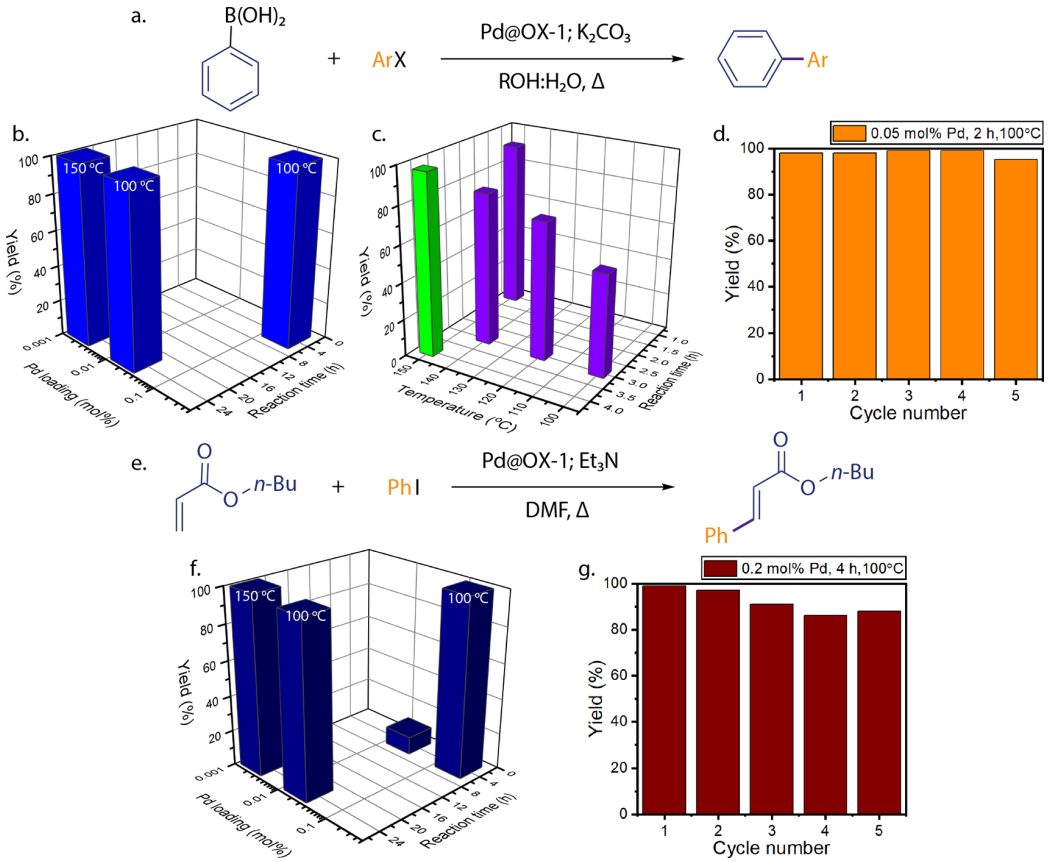

Figure 4. Pd@OX-1 catalytic performance in the Suzuki and Heck reactions. Model Suzuki reaction (a); variation of Pd loading for the reaction, ArX = PhI, ROH = MeOH (b); optimization of the reaction conditions, ArX = 4-bromoanisole with 0.002 mol % of Pd, ROH = *i*-PrOH (c); recycling of the material, ArX = PhI with 0.05 mol % of Pd at 100 °C, ROH = *i*-PrOH (d). Model Heck reaction (e); variation of Pd loading (f); recycling of the material, 0.2 mol % of Pd at 100 °C (g). This data is given in table form in the Supporting Information.

peak, shown in Figure 2d. The significantly lower frequency (<700 cm^{-1}) changes in INS spectra can be attributed to the changes in morphology of the crystals discussed above. These INS spectra therefore suggest that most modes in Pd@OX-1 composites are not significantly affected in the presence of Pd. The IR spectra, however, identify the BDC linkers of OX-1 as primary interaction sites between Pd guests and the host framework. The BDC linkers are thus the most likely active sites for attachment of Pd species in the Pd@OX-1 composite system.

Catalytic Performance of Guest Pd Species. Catalytic performance of 0.2 wt % Pd@OX-1 was studied in the Suzuki cross-coupling and the Heck arylation reactions, as they are well-known to be efficiently catalyzed by multiple palladium species.[26,27,29] All catalytic studies were performed under air in order to examine the robustness of the material.

In the Suzuki coupling of phenylboronic acid with iodobenzene (Figure 4a), catalyst activity was studied by decreasing the Pd loading from 0.2 mol % down to 0.002 mol %, where the latter corresponds to 20 ppm loading relative to PhI. The reaction was conducted in *i*-PrOH:H_2O (1:1) media and the product formation was analyzed by GC-MS. In all three cases >99% quantitative yields of biphenyl were reached (Figure 4b). Because of the high yields with PhI we used Ar-X, which is of lower reactivity, to address the material activity: 4-bromoanisole with 20 ppm catalyst loading. After 3 h of the reaction at 100, 120, and 140 °C, the product yield grew from 55% up to 82%. Moreover at 150 °C 91% yield was achieved already after 1 h, and after 4 h reached 97% of the 4-methoxybiphenyl product (Figure 4c). Following these results, preliminary scope studies were conducted, using 0.05 mol % of Pd at 100 °C. Both aryl iodides and bromides gave yields from good to excellent (see the SI). Electron properties of the substituents in aryl halide or aryl boronic acid have no significant effect on the outcome of the reaction. Steric bulkiness provided by the ortho-substituent (2-iodobenzaldehide) also did not affect an excellent product yield.

Even though visually the microstructure of the catalyst material changed after the reaction, seeming to be more agglomerated, we have analyzed the possibility of catalyst recycling with PhI, which is usually difficult because the freed iodide species in the solution are known to poison heterogeneous catalysts. The reaction was stopped after 2 h (98% yield), material was centrifuged, washed, and reused for another four cycles without significant loss of activity (see Figure 4d).

Next, the catalyst behavior in the Heck reaction was studied (Figure 4e). The approach was similar, butyl acrylate arylation with PhI was investigated with decreasing Pd loading. The outcome was roughly the same as for the Suzuki coupling. Butyl cinnamate was obtained with >99% yield after 24 h at 150 °C with only 20 ppm of Pd (Figure 4f). Although the catalyst was active toward iodide, when switching to 4-bromoanisole only traces of the reaction product were detected

DOI: 10.1021/acssuschemeng.8b05843
ACS Sustainable Chem. Eng. 2019, 7, 5875−5885

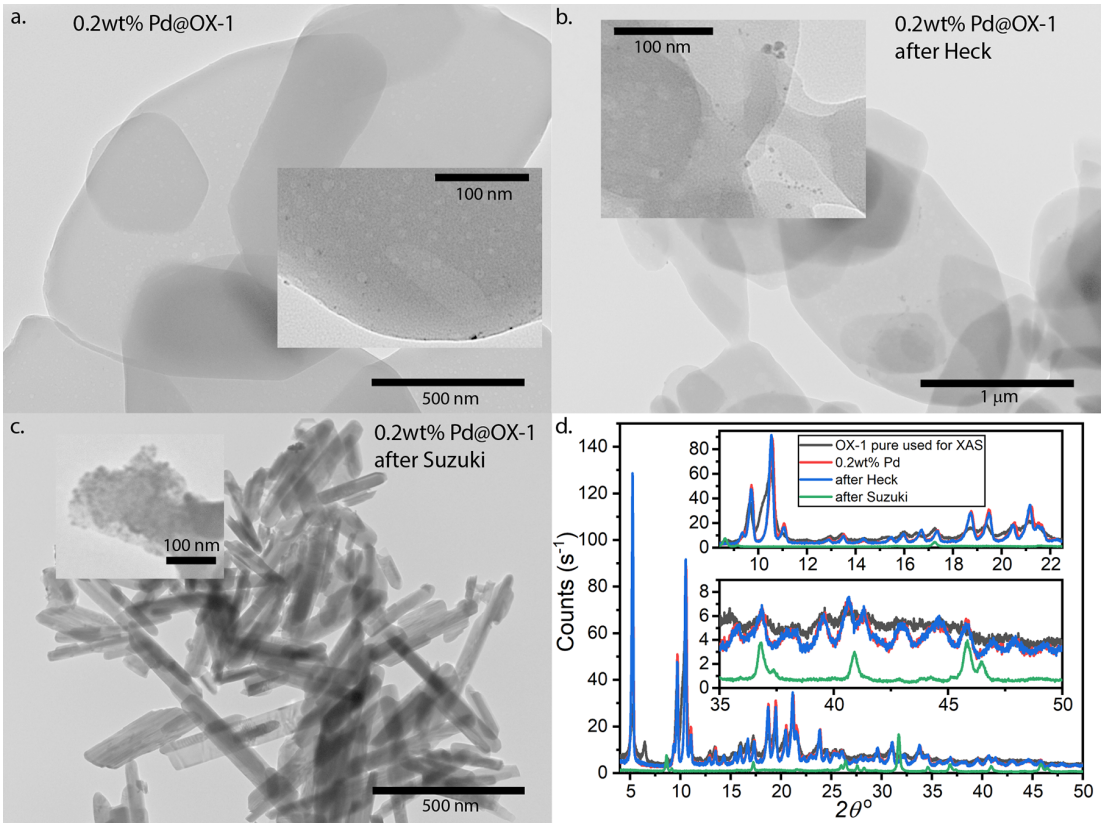

Figure 5. TEM images of (a) as synthesized Pd@OX-1 crystals and the same crystals after the (b) Heck and (c) Suzuki reactions. (d) XRD patterns for of the same set of samples.

after 24 h at an elevated temperature of 180 °C for either butyl acrylate or styrene. However, as with Suzuki coupling, the material could be recycled for five times, showing only slight loss of activity for PhI conversion (Figure 4g). Even though the medium in which the Heck reaction is performed is strikingly similar to the medium in which Pd@OX-1 is synthesized (DMF, Et_3N), the MOF appeared visually unchanged after the reaction except a slight change in color. Substrate scope was evaluated for the Heck reaction. Yields from good to excellent were obtained for all substrates (see the SI) with either electron withdrawing or electron donating groups. Utilization of an ortho-substituted iodotoluene resulted in lower yield of 81%. Comparing different acrylates we have observed that longer chain provides higher yield (Me- 84%, Et- 87%, *n*-Bu- 98%); while with increasing steric bulkiness the yield of the product was slightly lowered (*t*-Bu- 92%).

This ensemble of results demonstrates the high catalytic activity of Pd@OX-1 in a broad variety of conditions, as well as retainment of catalytic properties after both the Suzuki coupling and the Heck reactions.

Local Structure and Persistence of Active Sites. In recent decades diverse catalytic applications of Pd nanoparticles in cross-coupling reactions were facilitated by release of highly active Pd species to solution via leaching.[19] However, leaching of Pd species to solution often leads to dramatic loss of catalytic activity on the next cycle due to metal losses. Recapture of metal species from solution back to the surface of support after completing the catalytic process is the key challenge for retaining activity and avoiding contamination with palladium traces. Support materials do not routinely retain the ability to recapture metal species from solution after catalytic transformation under harsh conditions, which cause significant reconstruction of their surfaces. Thus, the observed performance of the material developed here prompted us to conduct more detailed characterization.

Pd@OX-1 owes its good catalytic performance and the possibility of recycling the material to the structure and persistence of its BDC active sites for Pd attachment. These are studied by probing the structure and local environments of Zn centers of OX-1 and of the various Pd species.

TEM imaging detects the presence of fine scale Pd nanoparticles on as synthesized 0.2 wt % Pd@OX-1 crystals (Figure 5a) with a size range of ca. 2−5 nm. Smaller particles were not detected at this microscope's resolution. After the Heck reaction (see the SI for reaction details) the morphology of the crystals appears to be unchanged, but most of the Pd nanoparticles appear to have grown in size, with particles as large as 10 nm (Figure 5b). After the Suzuki reaction (see the SI for reaction details), however, the shape of the recovered crystals changes dramatically to oblong particles. The size of Pd nanoparticles became even larger than in the case of the Heck reaction reaching 15−20 nm, as seen in TEM images (Figure 5c). XRD measurements (Figure 5d) reveal that crystal structure of Pd@OX-1 does not change during the Heck reaction but is completely different after the Suzuki reaction. This is remarkable: not only can OX-1 survive in DMF at 100 °C for at least 4 h for the Heck reaction and recapture[26,51−55] the active Pd species, but even after a dramatic change in microstructure during the Suzuki reaction it retains the Pd species and is still active in following cycles. To the best of our

DOI: 10.1021/acssuschemeng.8b05843
ACS Sustainable Chem. Eng. 2019, 7, 5875−5885

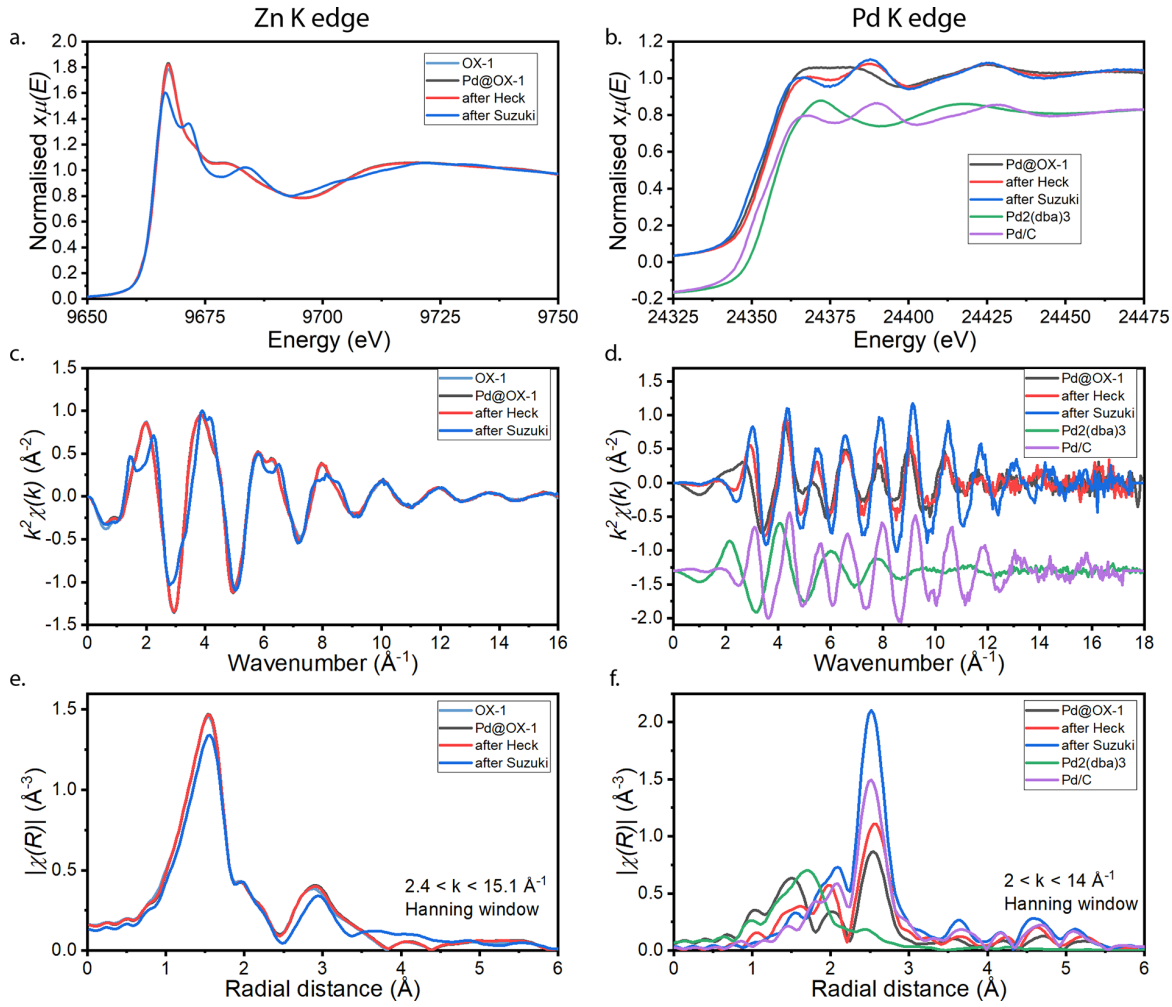

Figure 6. X-ray absorption spectra at the Zn (a, c, e) and Pd (b, d, f) K-edge of pure OX-1, pristine 0.2 wt % Pd@OX-1, Pd@OX-1 after the Heck and Suzuki reactions, of $Pd_2(dba)_3$ crystals and of Pd nanoparticles on graphite. In panels b and d, the spectra of $Pd_2(dba)_3$ and Pd/C have been shifted vertically for sake of comparison. Data processing and fitting were done in Demeter.[50]

knowledge this is a rare example of Pd recapture after total reconstruction of the material.

X-ray absorption spectroscopy (XAS) experiments were performed at the B18 beamline[56] of Diamond Light Source to study the possible changes in OX-1 crystal structure, as well as the structure and location of the attached Pd species, with results shown in Figure 6. X-ray absorption near edge structure (XANES) and extended X-ray absorption fine structure (EXAFS) data were collected at the Zn and Pd K-edges for the 0.2 wt % Pd@OX-1 as synthesized sample, a sample that was used to catalyze the Heck reaction, and a sample that was used to catalyze the Suzuki reaction. Moreover, precursor $Pd_2(dba)_3$ crystals and a sample of Pd nanoparticles on graphite[57] derived from $Pd_2(dba)_3$ were measured at the Pd K-edge for reference. This XAS data reflects the local structure around Zn and Pd atoms in the Pd@OX-1 system.

Zn K-edge measurements reveal that the introduction of $Pd_2(dba)_3$ into the synthesis does not change the framework structure around the Zn centers of OX-1. The spectra for OX-1 and Pd@OX-1 coincide almost exactly. There is only a slight increase of the white-line intensity when loading Pd into the host framework. This can be ascribed to a subtle enhancement of the localization of the final electronic states of Zn. This difference is negligible in the EXAFS signal. Thus, the local structure around Zn can be considered not affected by the loading of Pd.

Zn K-edge data further shows that the Zn environment of Pd@OX-1 does not change at all during the Heck reaction, confirming TEM and XRD observations discussed above. During the Suzuki reaction, however, the Zn environment is significantly altered: the profile of the XANES changes drastically becoming more structured. On the other hand, the pseudo-radial distribution function of the sample after the Suzuki reaction, in particular the first coordination shell is similar to the one obtained for the pristine Pd@OX-1 sample, meaning that the short-range order appears to be preserved. The changes in the XANES may be due to distortions in the bond angles which influences mainly the multiple scattering contributions. Indeed, the EXAFS signal for the sample after Suzuki reaction is more complex than the one for the original compound. This again confirms TEM and XRD observations and identifies this new structure as a new MOF-type material with long-range periodicity with a consistent local environment.

Pd K-edge data, Figure 6b, d, f, shows that the XANES of the samples after catalytic reactions are similar to the one

DOI: 10.1021/acssuschemeng.8b05843
ACS Sustainable Chem. Eng. 2019, 7, 5875−5885

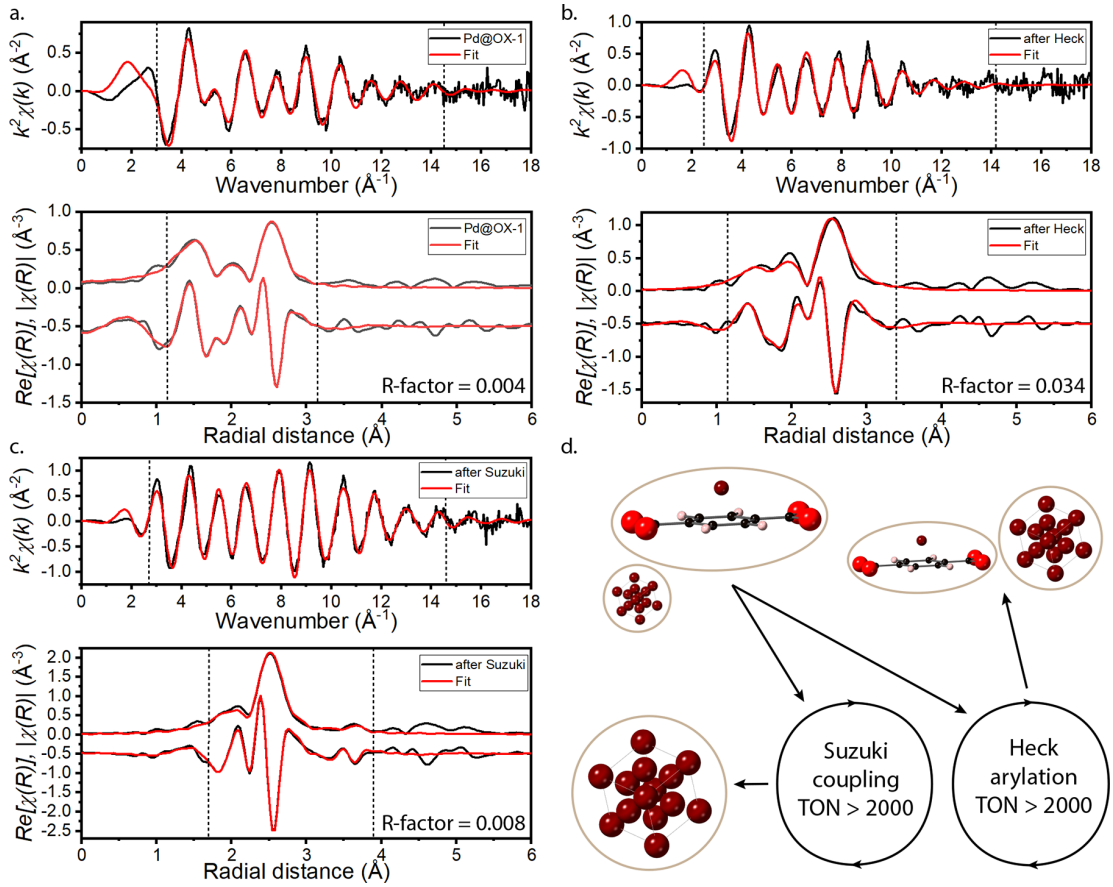

Figure 7. Fitting of EXAFS spectra for the as synthesized (a) 0.2 wt % Pd@OX-1, (b) Pd@OX-1 after the Heck reaction, and (c) Pd@OX-1 after the Suzuki reaction using models of Pd environments given in d. The "turn over number" (TON) is defined as the number of reactions catalyzed per Pd atom. Data processing and fitting were done in Demeter.[50]

obtained from the pristine Pd@OX-1 sample. The only difference is that the broad white-line of the pristine sample, characteristic of low order environments, splits into two structures after the reaction. This XANES profile with the two structures is very similar to the one obtained for the Pd/C sample which agrees with the fact of having larger Pd nanoparticles than the pristine sample.

The model used for performing the fitting analysis of the EXAFS data considered the Pd−C scattering path to the carbon atoms of benzene rings on BDC linkers, where Pd is assumed to be equidistant from all six members of the ring, and the Pd−Pd scattering paths characteristic of the face-centered cubic (FCC) Pd bulk. The fits can be seen in Figure 7, and the results from the fit can be found in Table S3 of the Supporting Information. The model seems to agree reasonably well with the experimental data despite its simplicity. From the fit we obtain a very low coordination number of Pd in as-synthesized Pd@OX-1, which suggests that the clusters of Pd inside the composite are very small, reflecting that a very high number of Pd atoms belong to surfaces of Pd particles. We reasoned that the as-synthesized Pd@OX-1 contains atomic Pd and Pd in small clusters coordinated to the π-system of the benzene rings of BDC linkers. Only a small number of particles are as big as those seen in the TEM images, while most of the Pd in the sample is not resolved. After both catalytic reactions, the coordination number of the Pd−Pd contribution increases, which indicates that the size of Pd nanoparticles has grown, in agreement with the TEM images. In the case of the after Suzuki sample in particular, the contribution of the Pd on the ligand component of the model was found to be negligible, so it was excluded from the fit.

Some recent results[21,22] also show that a shift to lower energy and a sharpening of the first near-edge peak of the XANES region are indicative of palladium hydride formation. In addition, this hydrogen bonding is accompanied by an elongation of the Pd−Pd distance (see Table S3). It is thus possible that during the Suzuki reaction some heteroatom insertion of hydrogen into the Pd nanoparticles may take place.

CONCLUSIONS

This paper presents a method of rapid *in situ* functionalization of OX-1 metal−organic nanosheets with catalytically active Pd species, obtained via a one-step one-pot supramolecular synthesis route. The loading of Pd can be controlled by adjusting the amount of $Pd_2(dba)_3$ added to the synthesis. The resulting Pd@OX-1 composite crystals contain predominantly atomic and small cluster Pd species, which selectively reside on benzene rings of the BDC linkers. The composites are shown to efficiently catalyze the Suzuki coupling and the Heck arylation reactions under a variety of conditions. The material retains the ability to recapture active Pd species during the reactions, which is not a routine property of common substrates for Pd nanoparticles. This enables the demonstrated potential for Pd@OX-1 to be recycled in reaction cycles of

DOI: 10.1021/acssuschemeng.8b05843
ACS Sustainable Chem. Eng. 2019, 7, 5875−5885

either type without loss of activity. More detailed studies are warranted to fully explore catalytic potential of the developed material as follow-on work, to systematically investigate the influence of various reaction conditions and substrates, among others. Undoubtedly, with its variety of Pd species and tunability of Pd loading, Pd@OX-1 shows promise as an attractive system for further study, with potential industrial applications in organic synthesis.

■ ASSOCIATED CONTENT

Supporting Information

The Supporting Information is available free of charge on the ACS Publications website at DOI: 10.1021/acssuschemeng.8b05843.

Experimental methods, additional XRD data, IR spectroscopy dielectric functions, and X-ray absorption spectroscopy analysis (PDF)

■ AUTHOR INFORMATION

Corresponding Authors

*Email: val@ioc.ac.ru (V.P.A.).
*Email: jin-chong.tan@eng.ox.ac.uk (J.C.T.).

ORCID

Dmitry B. Eremin: 0000-0003-2946-5293
Valentine P. Ananikov: 0000-0002-6447-557X
Jin-Chong Tan: 0000-0002-5770-408X

Author Contributions

⊥These authors contributed equally to this work.

Funding

The research in the MMC Lab (J.C.T.) was supported by the ERC Consolidator Grant—PROMOFS under the grant agreement 771575—and the EPSRC grant no. EP/N014960/1. Catalytic performance investigation (V.P.A.) was supported by the Russian Science Foundation (RSF Grant 14-50-00126).

Notes

The authors declare no competing financial interest.

■ ACKNOWLEDGMENTS

We acknowledge the Diamond Light Source for beamtime no. SM14902 at B22 MIRIAM and beamtime no. SP17146 in B18. We thank the ISIS facility for the provision of neutron beamtime no. RB1810348 on the TOSCA spectrometer. We are grateful to the ISIS Rutherford Appleton Laboratory, especially Dr. Gavin Stenning and Dr. Marek Jura at the R53 Materials Characterization Laboratory for access to XRF and XRD. We thank the Research Complex at Harwell (RCaH) for providing access to materials characterization facilities.

■ REFERENCES

(1) Hendon, C. H.; Rieth, A. J.; Korzynski, M. D.; Dinca, M. Grand Challenges and Future Opportunities for Metal-Organic Frameworks. *ACS Cent. Sci.* **2017**, *3* (6), 554−563.

(2) Dolgopolova, E. A.; Shustova, N. B. Metal-organic framework photophysics: Optoelectronic devices, photoswitches, sensors, and photocatalysts. *MRS Bull.* **2016**, *41* (11), 890−895.

(3) Zhu, L.; Liu, X. Q.; Jiang, H. L.; Sun, L. B. Metal-Organic Frameworks for Heterogeneous Basic Catalysis. *Chem. Rev.* **2017**, *117* (12), 8129−8176.

(4) Chughtai, A. H.; Ahmad, N.; Younus, H. A.; Laypkov, A.; Verpoort, F. Metal-organic frameworks: versatile heterogeneous catalysts for efficient catalytic organic transformations. *Chem. Soc. Rev.* **2015**, *44* (19), 6804−6852.

(5) Lee, J.; Farha, O. K.; Roberts, J.; Scheidt, K. A.; Nguyen, S. T.; Hupp, J. T. Metal-organic framework materials as catalysts. *Chem. Soc. Rev.* **2009**, *38* (5), 1450−1460.

(6) Gascon, J.; Corma, A.; Kapteijn, F.; Llabrés i Xamena, F. X. Metal Organic Framework Catalysis: Quo vadis? *ACS Catal.* **2014**, *4* (2), 361−378.

(7) Vermoortele, F.; Vandichel, M.; Van de Voorde, B.; Ameloot, R.; Waroquier, M.; Van Speybroeck, V.; De Vos, D. E. Electronic effects of linker substitution on Lewis acid catalysis with metal-organic frameworks. *Angew. Chem., Int. Ed.* **2012**, *51* (20), 4887−4890.

(8) Vermoortele, F.; Ameloot, R.; Alaerts, L.; Matthessen, R.; Carlier, B.; Fernandez, E. V. R.; Gascon, J.; Kapteijn, F.; De Vos, D. E. Tuning the catalytic performance of metal-organic frameworks in fine chemistry by active site engineering. *J. Mater. Chem.* **2012**, *22* (20), 10313−10321.

(9) Zhu, Q. L.; Xu, Q. Immobilization of Ultrafine Metal Nanoparticles to High-Surface-Area Materials and Their Catalytic Applications. *Chem.* **2016**, *1* (2), 220−245.

(10) Mehta, J. P.; Tian, T.; Zeng, Z. X.; Divitini, G.; Connolly, B. M.; Midgley, P. A.; Tan, J. C.; Fairen-Jimenez, D.; Wheatley, A. E. H. Sol-Gel Synthesis of Robust Metal-Organic Frameworks for Nanoparticle Encapsulation. *Adv. Funct. Mater.* **2018**, *28* (8), No. e1705588.

(11) Zhao, M.; Lu, Q.; Ma, Q.; Zhang, H. Two-Dimensional Metal-Organic Framework Nanosheets. *Small Methods* **2017**, *1* (1−2), 1600030.

(12) Pustovarenko, A.; Goesten, M. G.; Sachdeva, S.; Shan, M.; Amghouz, Z.; Belmabkhout, Y.; Dikhtiarenko, A.; Rodenas, T.; Keskin, D.; Voets, I. K.; Weckhuysen, B. M.; Eddaoudi, M.; de Smet, L.; Sudholter, E. J. R.; Kapteijn, F.; Seoane, B.; Gascon, J. Nanosheets of Nonlayered Aluminum Metal-Organic Frameworks through a Surfactant-Assisted Method. *Adv. Mater.* **2018**, *30* (26), No. e1707234.

(13) Chaudhari, A. K.; Tan, J. C. Mechanochromic MOF nanoplates: spatial molecular isolation of light-emitting guests in a sodalite framework structure. *Nanoscale* **2018**, *10* (8), 3953−3960.

(14) Osada, M.; Sasaki, T. Two-dimensional dielectric nanosheets: novel nanoelectronics from nanocrystal building blocks. *Adv. Mater.* **2012**, *24* (2), 210−228.

(15) Mas-Balleste, R.; Gomez-Navarro, C.; Gomez-Herrero, J.; Zamora, F. 2D materials: to graphene and beyond. *Nanoscale* **2011**, *3* (1), 20−30.

(16) He, T.; Ni, B.; Zhang, S.; Gong, Y.; Wang, H.; Gu, L.; Zhuang, J.; Hu, W.; Wang, X. Ultrathin 2D Zirconium Metal-Organic Framework Nanosheets: Preparation and Application in Photocatalysis. *Small* **2018**, *14* (16), No. e1703929.

(17) Chaudhari, A. K.; Kim, H. J.; Han, I.; Tan, J. C. Optochemically Responsive 2D Nanosheets of a 3D Metal-Organic Framework Material. *Adv. Mater.* **2017**, *29* (27), No. e1701463.

(18) Allendorf, M. D.; Medishetty, R.; Fischer, R. A. Guest molecules as a design element for metal-organic frameworks. *MRS Bull.* **2016**, *41* (11), 865−869.

(19) Balanta, A.; Godard, C.; Claver, C. Pd nanoparticles for C-C coupling reactions. *Chem. Soc. Rev.* **2011**, *40* (10), 4973−5057.

(20) Trzeciak, A. M. Pd Nanoparticles for Coupling Reactions and Domino/Tandem Reactions. Wiley-VCH: Weinheim, Germany, 2016.

(21) Bugaev, A. L.; Guda, A. A.; Lazzarini, A.; Lomachenko, K. A.; Groppo, E.; Pellegrini, R.; Piovano, A.; Emerich, H.; Soldatov, A. V.; Bugaev, L. A.; Dmitriev, V. P.; van Bokhoven, J. A.; Lamberti, C. In situ formation of hydrides and carbides in palladium catalyst: When XANES is better than EXAFS and XRD. *Catal. Today* **2017**, *283*, 119−126.

(22) Bugaev, A. L.; Usoltsev, O. A.; Lazzarini, A.; Lomachenko, K. A.; Guda, A. A.; Pellegrini, R.; Carosso, M.; Vitillo, J. G.; Groppo, E.; van Bokhoven, J. A.; Soldatov, A. V.; Lamberti, C. Time-resolved operando studies of carbon supported Pd nanoparticles under

DOI: 10.1021/acssuschemeng.8b05843
ACS Sustainable Chem. Eng. 2019, 7, 5875−5885

hydrogenation reactions by X-ray diffraction and absorption. *Faraday Discuss.* **2018**, *208* (0), 187−205.
(23) Carosso, M.; Lazzarini, A.; Piovano, A.; Pellegrini, R.; Morandi, S.; Manzoli, M.; Vitillo, J. G.; Ruiz, M. J.; Lamberti, C.; Groppo, E. Looking for the active hydrogen species in a 5 wt% Pt/C catalyst: a challenge for inelastic neutron scattering. *Faraday Discuss.* **2018**, *208* (0), 227−242.
(24) Frenkel, A. I.; Yevick, A.; Cooper, C.; Vasic, R. Modeling the structure and composition of nanoparticles by extended X-ray absorption fine-structure spectroscopy. *Annu. Rev. Anal. Chem.* **2011**, *4*, 23−39.
(25) Lopes, C. W.; Cerrillo, J. L.; Palomares, A. E.; Rey, F.; Agostini, G. An in situ XAS study of the activation of precursor-dependent Pd nanoparticles. *Phys. Chem. Chem. Phys.* **2018**, *20* (18), 12700−12709.
(26) Eremin, D. B.; Ananikov, V. P. Understanding active species in catalytic transformations: From molecular catalysis to nanoparticles, leaching, "Cocktails" of catalysts and dynamic systems. *Coord. Chem. Rev.* **2017**, *346*, 2−19.
(27) Ananikov, V. P.; Beletskaya, I. P. Toward the Ideal Catalyst: From Atomic Centers to a "Cocktail" of Catalysts. *Organometallics* **2012**, *31* (5), 1595−1604.
(28) Fairlamb, I. J. S.; Lee, A. F. Fundamental Pd-0/Pd-II Redox Steps in Cross-coupling Reactions: Homogeneous, Hybrid Homogeneous-Heterogeneous to Heterogeneous Mechanistic Pathways for C-C Couplings. *C-H and C-X Bond Functionalization: Transition Metal Mediation; RSC Catal. Ser.* **2013**, *11*, 72−107.
(29) Kashin, A. S.; Ananikov, V. P. Catalytic C-C and C-heteroatom bond formation reactions: in situ generated or preformed catalysts? Complicated mechanistic picture behind well-known experimental procedures. *J. Org. Chem.* **2013**, *78* (22), 11117−11125.
(30) Trzeciak, A. M.; Ziółkowski, J. J. Monomolecular, nanosized and heterogenized palladium catalysts for the Heck reaction. *Coord. Chem. Rev.* **2007**, *251* (9−10), 1281−1293.
(31) Ranocchiari, M.; van Bokhoven, J. A. Catalysis by metal-organic frameworks: fundamentals and opportunities. *Phys. Chem. Chem. Phys.* **2011**, *13* (14), 6388−6396.
(32) Fortea-Perez, F. R.; Mon, M.; Ferrando-Soria, J.; Boronat, M.; Leyva-Perez, A.; Corma, A.; Herrera, J. M.; Osadchii, D.; Gascon, J.; Armentano, D.; Pardo, E. The MOF-driven synthesis of supported palladium clusters with catalytic activity for carbene-mediated chemistry. *Nat. Mater.* **2017**, *16* (7), 760−766.
(33) Liu, J.; Ye, J.; Li, Z.; Otake, K. I.; Liao, Y.; Peters, A. W.; Noh, H.; Truhlar, D. G.; Gagliardi, L.; Cramer, C. J.; Farha, O. K.; Hupp, J. T. Beyond the Active Site: Tuning the Activity and Selectivity of a Metal-Organic Framework-Supported Ni Catalyst for Ethylene Dimerization. *J. Am. Chem. Soc.* **2018**, *140* (36), 11174−11178.
(34) Pascanu, V.; Yao, Q.; Bermejo Gomez, A.; Gustafsson, M.; Yun, Y.; Wan, W.; Samain, L.; Zou, X.; Martin-Matute, B. Sustainable catalysis: rational Pd loading on MIL-101Cr-NH_2 for more efficient and recyclable Suzuki-Miyaura reactions. *Chem. - Eur. J.* **2013**, *19* (51), 17483−17493.
(35) Metzger, E. D.; Brozek, C. K.; Comito, R. J.; Dincă, M. Selective Dimerization of Ethylene to 1-Butene with a Porous Catalyst. *ACS Cent. Sci.* **2016**, *2* (3), 148−153.
(36) Pascanu, V.; Bermejo Gómez, A.; Ayats, C.; Platero-Prats, A. E.; Carson, F.; Su, J.; Yao, Q.; Pericàs, M. A.; Zou, X.; Martín-Matute, B. n. Double-supported silica-metal−organic framework palladium nanocatalyst for the aerobic oxidation of alcohols under batch and continuous flow regimes. *ACS Catal.* **2015**, *5* (2), 472−479.
(37) Pascanu, V.; Hansen, P. R.; Bermejo Gomez, A.; Ayats, C.; Platero-Prats, A. E.; Johansson, M. J.; Pericas, M. A.; Martin-Matute, B. Highly functionalized biaryls via Suzuki-Miyaura cross-coupling catalyzed by Pd@MOF under batch and continuous flow regimes. *ChemSusChem* **2015**, *8* (1), 123−130.
(38) Yuan, N.; Pascanu, V.; Huang, Z.; Valiente, A.; Heidenreich, N.; Leubner, S.; Inge, A. K.; Gaar, J.; Stock, N.; Persson, I.; Martin-Matute, B.; Zou, X. Probing the Evolution of Palladium Species in Pd@MOF Catalysts during the Heck Coupling Reaction: An Operando X-ray Absorption Spectroscopy Study. *J. Am. Chem. Soc.* **2018**, *140* (26), 8206−8217.
(39) Puthiaraj, P.; Ahn, W.-S. Highly active palladium nanoparticles immobilized on NH_2-MIL-125 as efficient and recyclable catalysts for Suzuki−Miyaura cross coupling reaction. *Catal. Commun.* **2015**, *65*, 91−95.
(40) Shang, N.; Gao, S.; Zhou, X.; Feng, C.; Wang, Z.; Wang, C. Palladium nanoparticles encapsulated inside the pores of a metal−organic framework as a highly active catalyst for carbon−carbon cross-coupling. *RSC Adv.* **2014**, *4* (97), 54487−54493.
(41) Carson, F.; Pascanu, V.; Bermejo Gomez, A.; Zhang, Y.; Platero-Prats, A. E.; Zou, X.; Martin-Matute, B. Influence of the Base on Pd@MIL-101-NH_2 (Cr) as Catalyst for the Suzuki-Miyaura Cross-Coupling Reaction. *Chem. - Eur. J.* **2015**, *21* (30), 10896−10902.
(42) Dong, W.; Feng, C.; Zhang, L.; Shang, N.; Gao, S.; Wang, C.; Wang, Z. Pd@UiO-66: An Efficient Catalyst for Suzuki−Miyaura Coupling Reaction at Mild Condition. *Catal. Lett.* **2016**, *146* (1), 117−125.
(43) Bugaev, A. L.; Guda, A. A.; Lomachenko, K. A.; Kamyshova, E. G.; Soldatov, M. A.; Kaur, G.; Oien-Odegaard, S.; Braglia, L.; Lazzarini, A.; Manzoli, M.; Bordiga, S.; Olsbye, U.; Lillerud, K. P.; Soldatov, A. V.; Lamberti, C. Operando study of palladium nanoparticles inside UiO-67 MOF for catalytic hydrogenation of hydrocarbons. *Faraday Discuss.* **2018**, *208* (0), 287−306.
(44) Huang, Y.; Gao, S.; Liu, T.; Lü, J.; Lin, X.; Li, H.; Cao, R. Palladium Nanoparticles Supported on Mixed-Linker Metal-Organic Frameworks as Highly Active Catalysts for Heck Reactions. *ChemPlusChem* **2012**, *77* (2), 106−112.
(45) Zhang, L.; Su, Z.; Jiang, F.; Zhou, Y.; Xu, W.; Hong, M. Catalytic palladium nanoparticles supported on nanoscale MOFs: a highly active catalyst for Suzuki−Miyaura cross-coupling reaction. *Tetrahedron* **2013**, *69* (44), 9237−9244.
(46) Tahmasebi, S.; Mokhtari, J.; Naimi-Jamal, M. R.; Khosravi, A.; Panahi, L. One-step synthesis of Pd-NPs@Cu_2(BDC)$_2$DABCO as efficient heterogeneous catalyst for the Suzuki−Miyaura cross-coupling reaction. *J. Organomet. Chem.* **2017**, *853*, 35−41.
(47) Dong, W.; Zhang, L.; Wang, C.; Feng, C.; Shang, N.; Gao, S.; Wang, C. Palladium nanoparticles embedded in metal−organic framework derived porous carbon: synthesis and application for efficient Suzuki−Miyaura coupling reactions. *RSC Adv.* **2016**, *6* (43), 37118−37123.
(48) Titov, K.; Zeng, Z.; Ryder, M. R.; Chaudhari, A. K.; Civalleri, B.; Kelley, C. S.; Frogley, M. D.; Cinque, G.; Tan, J. C. Probing Dielectric Properties of Metal-Organic Frameworks: MIL-53(Al) as a Model System for Theoretical Predictions and Experimental Measurements via Synchrotron Far- and Mid-Infrared Spectroscopy. *J. Phys. Chem. Lett.* **2017**, *8* (20), 5035−5040.
(49) Civalleri, B.; Napoli, F.; Noel, Y.; Roetti, C.; Dovesi, R. Ab-initio prediction of materials properties with CRYSTAL: MOF-5 as a case study. *CrystEngComm* **2006**, *8* (5), 364−371.
(50) Ravel, B.; Newville, M. ATHENA, ARTEMIS, HEPHAESTUS: data analysis for X-ray absorption spectroscopy using IFEFFIT. *J. Synchrotron Radiat.* **2005**, *12* (4), 537−541.
(51) Zhao, F.; Bhanage, B. M.; Shirai, M.; Arai, M. Heck Reactions of Iodobenzene and Methyl Acrylate with Conventional Supported Palladium Catalysts in the Presence of Organic and/or Inorganic Bases without Ligands. *Chem. - Eur. J.* **2000**, *6* (5), 843−848.
(52) Borja, G.; Monge-Marcet, A.; Pleixats, R.; Parella, T.; Cattoen, X.; Man, M. W. C. Recyclable Hybrid Silica-Based Catalysts Derived from Pd-NHC Complexes for Suzuki, Heck and Sonogashira Reactions. *Eur. J. Org. Chem.* **2012**, *2012* (19), 3625−3635.
(53) Genelot, M.; Dufaud, V.; Djakovitch, L. Carbonylative Sonogashira Coupling in the Synthesis of Ynones: A Study of "Boomerang" Phenomena. *Adv. Synth. Catal.* **2013**, *355* (13), 2604−2616.
(54) Gruttadauria, M.; Giacalone, F.; Noto, R. "Release and catch" catalytic systems. *Green Chem.* **2013**, *15* (10), 2608−2618.
(55) Giacalone, F.; Campisciano, V.; Calabrese, C.; La Parola, V.; Syrgiannis, Z.; Prato, M.; Gruttadauria, M. Single-Walled Carbon

DOI: 10.1021/acssuschemeng.8b05843
ACS Sustainable Chem. Eng. 2019, 7, 5875−5885

Nanotube-Polyamidoamine Dendrimer Hybrids for Heterogeneous Catalysis. *ACS Nano* **2016**, *10* (4), 4627−36.
(56) Dent, A.; Cibin, G.; Ramos, S.; Smith, A.; Scott, S.; Varandas, L.; Pearson, M.; Krumpa, N.; Jones, C.; Robbins, P. In *B18: A core XAS spectroscopy beamline for Diamond*; Journal of Physics: Conference Series; IOP Publishing: 2009; p 012039.
(57) Pentsak, E. O.; Kashin, A. S.; Polynski, M. V.; Kvashnina, K. O.; Glatzel, P.; Ananikov, V. P. Spatial imaging of carbon reactivity centers in Pd/C catalytic systems. *Chem. Sci.* **2015**, *6* (6), 3302−3313.

NOTE ADDED AFTER ASAP PUBLICATION

This paper was published on the Web on March 1, 2019, with errors in Figures 4, 6, and 7. The corrected version was reposted on March 4, 2019.

DOI: 10.1021/acssuschemeng.8b05843
ACS Sustainable Chem. Eng. 2019, 7, 5875−5885